**Unlocking Discontinuous Residual Oil: A Pore-Scale Study on the Interaction of Swelling, Extraction, and Viscosity Reduction**

## Introduction

Carbon Capture, Utilization, and Storage (CCUS) is a vital strategy for reducing $CO_2$ emissions while meeting energy demands (Davoodi et al. 2023, Ren et al. 2022). Among various CCUS technologies, $CO_2$-enhanced oil recovery ($CO_2$-EOR) is particularly effective. It improves oil production and provides reliable geological storage for $CO_2$ (Al-Shargabi et al. 2022, Zhuang et al. 2024). During this process, multiple mechanisms—such as oil swelling, viscosity reduction, and light component extraction—play critical roles in mobilizing residual oil (Eyinla et al. 2023). While macro-scale recovery and storage potentials have been extensively quantified, the fundamental displacement efficiency is ultimately governed by complex gas-oil interactions at the pore scale.

Recent studies have used microfluidic experiments and pore-scale simulations to explore these processes (Alhosani et al. 2021, Guo et al. 2022, Shi et al. 2024, Wang et al. 2024). These investigations have provided valuable visual evidence of fluid distribution and phase behavior under various reservoir conditions (Zhang et al. 2025). However, traditional models often simplify the complex interactions between fluid flow and species diffusion. The neglect of dynamic mass transfer can lead to inaccurate predictions of oil mobilization and gas storage capacity. While the Volume-of-Fluid (VOF) method combined with the Continuum Species Transfer (CST) approach has shown promise in tracking interfaces and mass transfer (Carrillo et al. 2020, Haroun et al. 2012, Maes and Soulaine 2020), it is still challenging to fully describe how swelling, extraction, and viscosity reduction together affect discontinuous residual oil at the pore scale.

In this work, we employ an advanced multiphase-multicomponent simulation model based on the VOF-CST approach to investigate the physics of discontinuous residual oil mobilization. Utilizing a 2D T-shaped dead-end pore model, this study first analyze how $CO_2$ diffusion, oil swelling, light component extraction and viscosity reduction work together to mobilize trapped oil during the gas injection process. Subsequently, we evaluate the displacement efficiency of $CO_2$ under water film conditions, specifically focusing on how $CO_2$ penetrates water barriers to reach and mobilize residual oil. The findings aim to provide a theoretical foundation for optimizing $CO_2$-EOR and storage performance in complex subsurface environments.

## Method

The VOF method is used to track the gas-oil interface. The distribution of the two phases is defined by the phase fraction $\alpha$. Consider the multi-component mass transfer, the governing equations are expressed as follows (Bothe and Fleckenstein 2013, Deising et al. 2016, Raeini et al. 2012):

$$\mathrm{div}\,\mathbf{u} = \dot{m}\left(\frac{1}{\rho_\mathrm{o}} - \frac{1}{\rho_\mathrm{g}}\right) \tag{1}$$

$$\partial_t(\rho\boldsymbol{u}) - \mathrm{div}\,\mathbf{S} = -\nabla p + \rho\boldsymbol{g} + \boldsymbol{f}_\Sigma \tag{2}$$

$$\partial_t\alpha + \mathrm{div}(\alpha\boldsymbol{u}) + \mathrm{div}(\alpha(1-\alpha)\boldsymbol{u}_\mathrm{r}) = \frac{\dot{m}}{\rho_\mathrm{o}} + \alpha\mathrm{div}(\boldsymbol{u}) \tag{3}$$

$$\partial_t c + \mathrm{div}(c\boldsymbol{u} + \boldsymbol{j}) = 0 \tag{4}$$

where $\boldsymbol{u}$ is the velocity. $\rho$ is the fluid density. $p$ is the pressure. $\mathbf{S} = \mu(\nabla\boldsymbol{u} + (\nabla\boldsymbol{u})^{\boldsymbol{T}})$ is the viscous stress tensor. $\mu$ is the dynamic viscosity. $\boldsymbol{g}$ is the gravity vector, and the gravity force. $\boldsymbol{f}_\Sigma$ is the capillary force which dominates the subsurface seepage processes. The interfacial tension $\sigma$ is considered constant throughout the simulation. $c$ is the species concentration. The diffusive flux $\boldsymbol{j} = -MD\nabla c = -D\nabla\rho$ can be modelled using Fick's law. $D$ is the molecular diffusivity and $M$ is the molar mass.
The gas solubility controlled by concentration jump at the interface, which is given by Henry's law with a constant coefficient $H$ (Haroun, Raynal and Legendre 2012, Marschall et al. 2012).

$$c_g = Hc_o \tag{5}$$

The concentration equation is resolved through a modified CST approach (Maes and Soulaine 2018). The diffusive flux $\mathbf{j}$ is consisted as the sum of original diffusive flux and an additional CST flux (Haroun et al. 2010).

$$\boldsymbol{j} = -\widehat{D}\nabla c + \boldsymbol{\Phi} \tag{6}$$

$$\boldsymbol{\Phi} = (\mathrm{H}-1)\,\widehat{D}\frac{c}{H\alpha + (1-\alpha)}\nabla\alpha \tag{7}$$

$$\widehat{\mathrm{D}} = \frac{H\alpha D_o + (1-\alpha)D_g}{H\alpha + (1-\alpha)} \tag{8}$$

where $\widehat{\mathrm{D}}$ is the equilibrium-based mean diffusion coefficient. The CST flux $\boldsymbol{\Phi}$ at the gas-fluid interface due to the concentration discontinuity limited by the solubility with different temperature and pressure conditions.

This volumetric mass transfer rate $\dot{\mathrm{m}}$ also should be calculated and re-assigned into the governing equations. The total interfacial mass transfer rate of the gas-oil system can be calculated as (Maes and Soulaine 2020),

$$\dot{m} = -\frac{\widehat{D}\nabla \mathrm{c} - \boldsymbol{\Phi}}{\alpha Y_{hc}} \cdot \nabla\alpha \tag{9}$$

where $Y_{hc}$ is the mole fraction of the solvent component (the heavy component) in oil.

An additional smoothed symmetric mass transfer term is added to control the effective interface movement. More details of source term calculation and the corresponding verification can be found in previous work (Zhang et al. 2026).

PVT test results show that changes in fluid composition consequently alter the wettability and interfacial tension between oil and gas (Sharbatian et al. 2018). Therefore, concentration-dependent models for contact angle and interfacial tension are required to describe the capillary-force variation under compositional effects. Assuming these parameters vary linearly with concentration, the $\boldsymbol{f}_\Sigma$ can be expressed as:

$$\boldsymbol{f}_\Sigma = \boldsymbol{f}_{\Sigma_{\min}} + (\boldsymbol{f}_{\Sigma_{\max}} - \boldsymbol{f}_{\Sigma_{\min}})\frac{\mathrm{c}_{\text{average}}}{\mathrm{c}_{\max}} \tag{10}$$

where $\mathrm{c}_{\text{average}}$ is the local average concentration. $\mathrm{c}_{\max}$ is the maximum concentration of dissolved gas, which is equal to the $CO_2$ solubility.

Similarly, a concentration-dependent viscosity model is implemented, where the oil phase viscosity decreases as $CO_2$ dissolves. The quarter-law mixing rule was introduced (Afshari et al. 2018, Afshari et al. 2020),

$$\mu_\mathrm{o}(c_g) = [\frac{c_\mathrm{g} - c_{\mathrm{g,ini}}}{c_{\mathrm{g,inj}} - c_{\mathrm{g,ini}}}\mu_\mathrm{g}^{-0.25} + \left(1 - \frac{c_\mathrm{g} - c_{\mathrm{g,ini}}}{c_{\mathrm{g,inj}} - c_{\mathrm{g,ini}}}\right)\mu_\mathrm{o}^{-0.25}]^{-4} \tag{11}$$

where $c_g$ denotes the $CO_2$ concentration. $c_{g,\mathrm{inj}}$ is the inlet concentration. $c_{g,\mathrm{ini}} = 0$ is the initial concentration of dissolved $CO_2$ in the oil phase.

## Coupled Mechanisms in T-shaped Dead-end Pore

The interaction between $CO_2$ and oil was first validated using a 2D micro-PVT model. The verified simulation parameters are shown in the ***Table 1***. Under 50°C and 11 MPa, a bidirectional mass transfer occurs: $CO_2$ dissolves into the oil (swelling and viscosity reduction), while light oil components are extracted into the gas phase. The simulations were conducted in a T-shaped dead-end pore which consists of a blind-ended pore (region A). $CO_2$ was injected from the left inlet with a fixed injection velocity of 5 mm/s. The model is assumed to be oil-wet (contact angle 60°) based on in-situ contact angle measurements (Blunt et al. 2021).

To quantify the impact of these mechanisms, three models were compared (***Figure 1*** ):

Model 1 (No mass transfer): $CO_2$ quickly bypasses the dead-end, leaving a residual oil saturation of 0.76.

Model 2 (Swelling & Extraction): Swelling creates a reverse velocity component at the interface, slowing down displacement and delaying snap-off. Even after snap-off, extraction continues to mobilize oil, improving recovery by 19.87% compared to Model 1.
Model 3 (Full Coupling): Adding viscosity reduction significantly enhances mobility. Using a power-law viscosity model, the recovery increases by 29.95% over Model 1, proving that accurate viscosity-concentration fitting is crucial for EOR assessment.

***Table 1*** *The fluid phase properties.*

| Phase | Density ($kg/m^3$) | Viscosity (Pa·s) | Interfacial tension (mN/m) | $CO_2$ Mole fraction (%) | $CO_2$ D ($m^2/s$) | $CO_2$ H | Light component Mole fraction (%) | Light component D ($m^2/s$) | Light component H | Heavy component Mole fraction (%) | Heavy component D ($m^2/s$) | Heavy component H |
|---|---|---|---|---|---|---|---|---|---|---|---|---|
| Gas | 502.6 | $3.6\times10^{-6}$ | 5 | 100 | $8\times10^{-7}$ | 1.9 | 0 | $1\times10^{-7}$ | 0.16 | 0 | / | 0 |
| Oil | 710.5 | $1.4\times10^{-4}$ | | 0 | $4\times10^{-8}$ | | 67.5 | $8\times10^{-9}$ | | 32.5 | $1\times10^{-9}$ | |

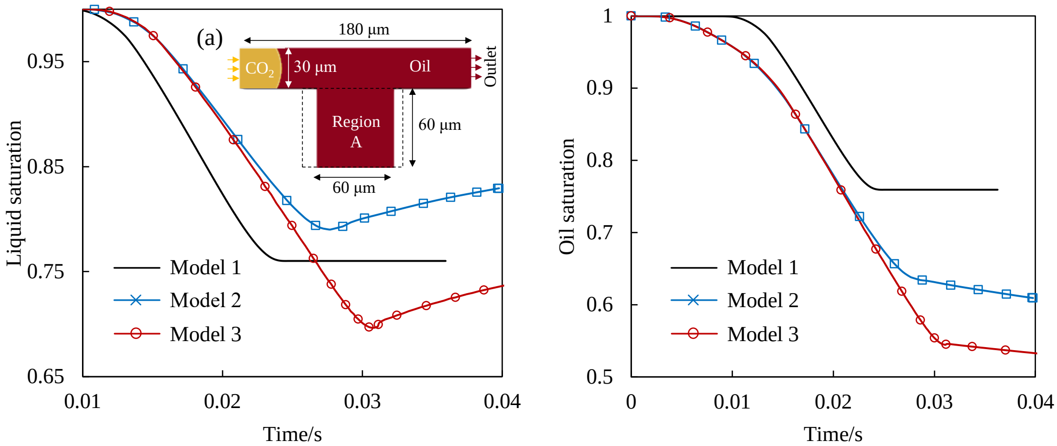

(b) (c)

***Figure 1*** *The liquid saturation curves (b) and oil saturation curves (c) with different models in a T-shaped dead-end pore (a).*

**Impact of Water on Mobilization Efficiency**

(1) Connate Water Conditions

In a water-wet T-pore with 33.5% initial water saturation, some CO2 dissolves into the water phase. This reduces the $CO_2$ concentration available for the oil phase by approximately 5%, leading to a 2.4% overestimation of recovery efficiency if water-solubility is ignored (***Figure 2***).

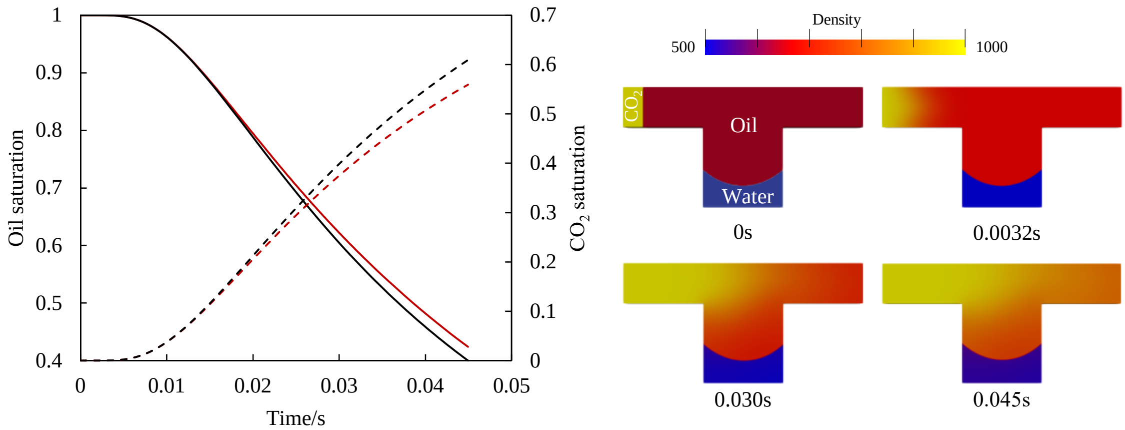

(a) (b)

***Figure 2*** *The saturation curves (a) and the fluid density variations (b) during miscible gas flooding.*

(2) Miscible Gas Injection after Waterflooding

A critical finding is the mobilization of residual oil trapped behind a water film. As shown in ***Figure 3***, the residual oil in the dead-end remains trapped without diffusion in water during $CO_2$ injection. The water phase then can be an intermediate medium under simulation considering diffusion in water. The dissolved gas front moves faster than the gas-water interface, reaching the trapped oil through the water phase. This triggers swelling and viscosity reduction before direct gas-oil contact. Eventually, the thinning water film ruptures, allowing the oil and gas to mix and be produced. The simulation shows that after mixing, light and medium components are extracted first, leaving a higher relative concentration of heavy components in the dead-end.

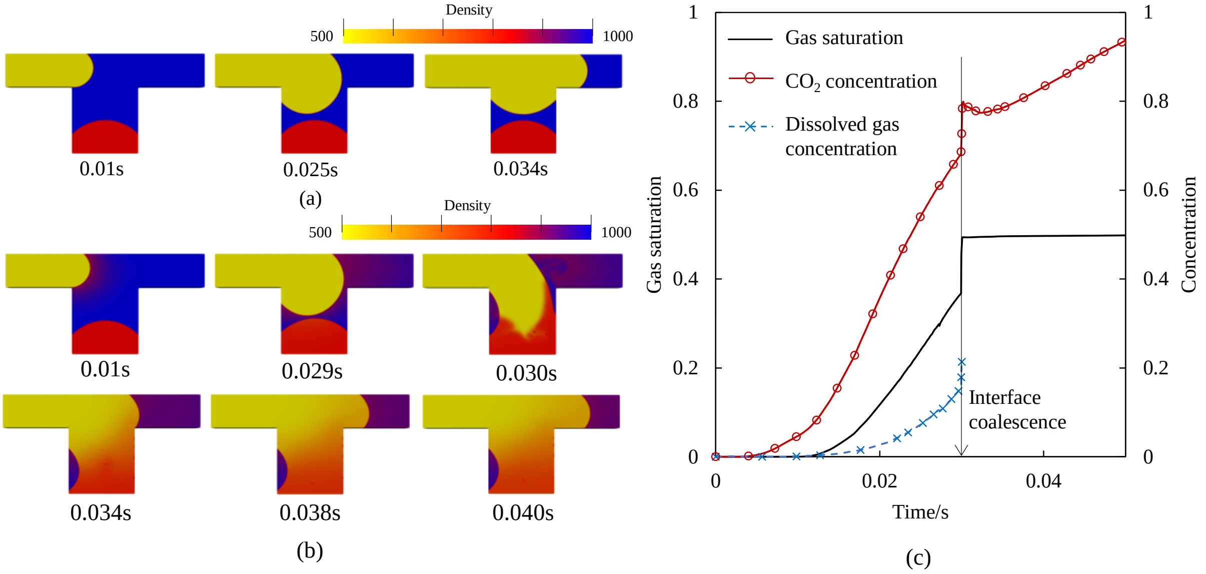


***Figure 3*** *The phase distribution evolution (simulation without gas diffusion (a) and simulation with gas diffusion (b) ) and the curves of gas saturation and dissolved gas concentration (c).*

## Conclusions

This study utilized a pore-scale VOF-CST model to investigate the mobilization of discontinuous residual oil during $CO_2$-EOR and storage. Here, we summarize the main findings:

- The mobilization of trapped oil is driven by the dynamic coupling of swelling, extraction, and viscosity reduction. Compared to gas displacement without diffusion, the extraction mechanism contributes to a 19.87% improvement in recovery. When further coupled with a power-law viscosity reduction model, the recovery efficiency increases by 29.95%, demonstrating that the significant reduction in oil viscosity due to dissolved CO2 is a key driver for EOR.
- In systems with connate water, the dissolution of $CO_2$ into the aqueous phase reduces the gas concentration available for the oil phase by approximately 5%. This leads to a 2.4% overestimation of recovery efficiency if the gas solubility in water is ignored.
- The water phase acts as a permeable medium for $CO_2$. Dissolved gas can diffuse through water films to reach trapped oil clusters, triggering swelling and mobilization even before direct gas-oil contact.

## Acknowledgements

We would like to express appreciation to the following financial support: National Key R&D Program of China (NO. 2023YFB4104200), the National Natural Science Foundation of China (No. U23A20595, 52034010, 52288101), National Key Research and Development Program of China (2022YFE0203400), Shandong Provincial Natural Science Foundation (ZR2024ZD17), Qingdao Natural Science Foundation (No. 23-2-1-230-zyyd-jch), the Fundamental Research Funds for the Central Universities (No. 23CX10004A), and Program for Changjiang Scholars and Innovative Research Team in University (IRT_16R69).

## References


Afshari, S., Hejazi, S. H. and Kantzas, A. [2018] Role of medium heterogeneity and viscosity contrast in miscible flow regimes and mixing zone growth: A computational pore-scale approach. Physical Review Fluids 3(5), 054501.

Afshari, S., Hejazi, S. H. and Kantzas, A. [2020] Pore-scale modeling of coupled thermal and solutal dispersion in double diffusive-advective flows through porous media. International Journal of Heat and Mass Transfer 147, 118730.

Al-Shargabi, M., Davoodi, S., Wood, D. A., Rukavishnikov, V. S. and Minaev, K. M. [2022] Carbon Dioxide Applications for Enhanced Oil Recovery Assisted by Nanoparticles: Recent Developments. ACS Omega 7(12), 9984-9994.

Alhosani, A., Bijeljic, B. and Blunt, M. J. [2021] Pore-Scale Imaging and Analysis of Wettability Order, Trapping and Displacement in Three-Phase Flow in Porous Media with Various Wettabilities. Transport in Porous Media 140(1), 59-84.

Blunt, M. J., Alhosani, A., Lin, Q., Scanziani, A. and Bijeljic, B. [2021] Determination of contact angles for three-phase flow in porous media using an energy balance. Journal of Colloid and Interface Science 582, 283-290.

Bothe, D. and Fleckenstein, S. [2013] A Volume-of-Fluid-based method for mass transfer processes at fluid particles. Chemical Engineering Science 101, 283-302.

Carrillo, F. J., Bourg, I. C. and Soulaine, C. [2020] Multiphase flow modeling in multiscale porous media: An open-source micro-continuum approach. Journal of Computational Physics: X 8, 100073.

Davoodi, S., Al-Shargabi, M., Wood, D. A., Rukavishnikov, V. S. and Minaev, K. M. [2023] Review of technological progress in carbon dioxide capture, storage, and utilization. Gas Science and Engineering 117, 205070.

Deising, D., Marschall, H. and Bothe, D. [2016] A unified single-field model framework for Volume-Of-Fluid simulations of interfacial species transfer applied to bubbly flows. Chemical Engineering Science 139, 173-195.

Eyinla, D. S., Leggett, S., Badrouchi, F., Emadi, H., Adamolekun, O. J. and Akinsanpe, O. T. [2023] A comprehensive review of the potential of rock properties alteration during $CO_2$ injection for EOR and storage. Fuel 353, 129219.

Guo, Y., Liu, F., Qiu, J., Xu, Z. and Bao, B. [2022] Microscopic transport and phase behaviors of $CO_2$ injection in heterogeneous formations using microfluidics. Energy 256, 124524.

Haroun, Y., Legendre, D. and Raynal, L. [2010] Volume of fluid method for interfacial reactive mass transfer: Application to stable liquid film. Chemical Engineering Science 65(10), 2896-2909.

Haroun, Y., Raynal, L. and Legendre, D. [2012] Mass transfer and liquid hold-up determination in structured packing by CFD. Chemical Engineering Science 75, 342-348.

Maes, J. and Soulaine, C. [2018] A new compressive scheme to simulate species transfer across fluid interfaces using the Volume-Of-Fluid method. Chemical Engineering Science 190, 405-418.

Maes, J. and Soulaine, C. [2020] A unified single-field Volume-of-Fluid-based formulation for multi-component interfacial transfer with local volume changes. Journal of Computational Physics 402, 109024.

Marschall, H., Hinterberger, K., Schüler, C., Habla, F. and Hinrichsen, O. [2012] Numerical simulation of species transfer across fluid interfaces in free-surface flows using OpenFOAM. Chemical Engineering Science 78, 111-127.

Raeini, A. Q., Blunt, M. J. and Bijeljic, B. [2012] Modelling two-phase flow in porous media at the pore scale using the volume-of-fluid method. Journal of Computational Physics 231(17), 5653-5668.

Ren, B., Male, F. and Duncan, I. J. [2022] Economic analysis of CCUS: Accelerated development for $CO_2$ EOR and storage in residual oil zones under the context of 45Q tax credit. Applied Energy 321, 119393.

Sharbatian, A., Abedini, A., Qi, Z. and Sinton, D. [2018] Full Characterization of $CO_2$-Oil Properties On-Chip: Solubility, Diffusivity, Extraction Pressure, Miscibility, and Contact Angle. Analytical chemistry 90 4, 2461-2467.

Shi, J., Tao, L., Guo, Y., He, X., Li, Y. and Bao, B. [2024] Visualization of $CO_2$-oil vanishing interface to determine minimum miscibility pressure using microfluidics. Fuel 362, 130876.

Wang, X., Li, S., Tong, B., Jiang, L., Lv, P., Zhang, Y. and Song, Y. [2024] Wettability and capillary behavior in a $CO_2$–oil–solid system under near-miscible conditions: A pore-scale study. Fuel 364, 131164.

Zhang, Q., Yang, Y., Zhang, L., Sun, H., Zhong, J., Zhang, K. and Yao, J. [2026] Improved single-field VOF method for interfacial mass transfer modeling: Application to $CO_2$-EOR and carbon sequestration in hydrocarbon reservoirs. International Journal of Heat and Mass Transfer 255, 127807.

Zhang, S., Sha, X., Wei, H., Chen, L. and Tao, W.-q. [2025] Microfluidic experimental study of CO2-water-oil three-phase flow in porous media under both immiscible and miscible conditions. International Communications in Heat and Mass Transfer 169, 109703.

Zhuang, X., Wang, W., Su, Y., Li, Y., Dai, Z. and Yuan, B. [2024] Spatio-temporal sequence prediction of $CO_2$ flooding and sequestration potential under geological and engineering uncertainties. Applied Energy 359, 122691.